Mon. Not. R. astr. Soc. (1986) **219,** 403–416

Spectroscopy of the QSOs Q0118−031 A, B, C★

J. G. Robertson *Anglo-Australian Observatory, PO Box 296, Epping, NSW 2121, Australia*

P. A. Shaver and J. Surdej† *European Southern Observatory, Karl-Schwarzschild-Str. 2, D-8046 Garching bei München, FRG*

J. P. Swings *Institute of Astrophysics, University of Liege, Avenue de Cointe, 5, B-4200 Cointe-Ougree, Belgium*

Accepted 1985 October 9. Received 1985 October 1

Summary. We present optical spectroscopy of the three quasars Q0118−031A, B, C. These objects form a triplet on the plane of the sky, with separations of 4′.8, 4′.9 and 0′.4. Their emission redshifts are 1.445 (A), 2.112 (B), and 1.165 (C). Low dispersion spectra (showing the emission lines) were obtained for all three objects, and intermediate dispersion spectra (resolution ~1.5 Å FWHM) were obtained for objects B and C, to search for absorption lines.

QSO B has a rich absorption line spectrum, with a very strong system at $z_{abs}=2.0192$ and another definite system at $z_{abs}=1.4648$. No absorption lines were found in our spectrum of Q0118−031C. Estimated column densities and velocity dispersions are given for the absorption systems in Q0118−031B. The one at $z_{abs}=1.4648$ is of particular interest because it differs by only $2400\pm250\,\mathrm{km\,s^{-1}}$ from the emission redshift of Q0118−031A. The projected spatial separation is 1.2 Mpc ($H_o=100\,\mathrm{km\,s^{-1}\,Mpc^{-1}}$, $\Omega=1$) so this absorption system may be due to material associated with a galaxy in a cluster which also contains QSO A. Although the probability of chance agreement of absorption and emission redshifts (to within $\pm2400\,\mathrm{km\,s^{-1}}$) is not negligible, this is the second example of such associated absorption (the other is Q1228+076/7) and the fourth if we count also two cases in which the velocity and spatial separations are much smaller (more appropriate to a disc or halo surrounding the lower redshift QSO itself). Therefore the evidence is steadily building up that associated absorption does show that quasars are located in regions of higher than average matter density.

★ Based on observations made at the Anglo–Australian Telescope, the Multiple Mirror Telescope (operated by the University of Arizona and the Smithsonian Institution) and the European Southern Observatory at La Silla.

† Also, Chercheur Qualifié au Fonds National de la Recherche Scientifique (Belgium).

1 Introduction

The study of pairs of quasars which lie close together on the plane of the sky (but which may be at very different redshifts) can give significant information about the size and location of the clouds causing the narrow absorption lines in QSO spectra. Previous observations of such pairs have shown that two rather distinct relationships can occur between the spectra of the two objects:

(i) Absorption may be seen at essentially the same redshift in both spectra. This is referred to as common absorption and is interpreted as due to either a single cloud or two physically related clouds along the two neighbouring lines of sight. Discounting the gravitational lens QSO pairs (where the spatial separation of the two lines of sight is very small), common absorption is not often observed. Only Q0307−195A, B, separated by 58″ at $z=2.144, 2.122$ (Shaver & Robertson 1983a) show common absorption of this type.

(ii) Absorption may be seen in the higher redshift (background) QSO at a redshift ($z_{\mathrm{abs,H}}$) close to the emission redshift ($z_{\mathrm{em,L}}$) of the other, lower redshift member. We call this associated absorption and interpret it as being due to material physically associated with the lower redshift (foreground) QSO – either a halo of a galaxy in a cluster which also contains the foreground QSO, or a halo surrounding the foreground QSO itself (depending on the spatial and velocity separations between the QSO and the absorbing region concerned).

At present there are three known cases of associated absorption: Q0028+003/0029+003 (Shaver, Boksenberg & Robertson 1982; projected spatial separation 260 kpc ($H_o=100\,\mathrm{km\,s^{-1}}$ $\mathrm{Mpc^{-1}}$, $\Omega=1$), velocity separation $\Delta(z_{\mathrm{abs,H}}:z_{\mathrm{em,L}})\equiv 190\,\mathrm{km\,s^{-1}}$), Q0307−195A, B (Shaver & Robertson 1983a; separations 230 kpc and $80\,\mathrm{km\,s^{-1}}$) and Q1228+076/1228+077 (Robertson & Shaver 1983; separations 840 kpc and $2000\,\mathrm{km\,s^{-1}}$). The very close pair Q1548+114A, B was previously thought to exhibit associated absorption (Burbidge *et al.* 1977) but the associated absorption system claimed by those authors has been shown not to exist by Shaver & Robertson (1985). In the case of Q0028+003/0029+003 and Q0307−195A, B the small spatial and velocity separations between the absorber and foreground QSO suggest that the absorption may be due to a disc or halo surrounding the QSO itself, while for Q1228+076/1228+077 the separations are consistent with absorption by material in a cluster of galaxies which also contains the lower redshift QSO. The observations to be presented here show that Q0118−031A, B is another pair exhibiting associated absorption, similar in character to that in Q1228+076/1228+077.

This paper presents observations of three QSOs which form a triplet in the plane of the sky, Q0118−031A, B, C. Low dispersion (emission line) spectroscopy is given for all three objects, and intermediate dispersion spectroscopy for Q0118−031B and C. A detailed discussion is given of the rich absorption spectrum of Q0118−031B.

These QSOs were found in a UVX survey of a field centred on NGC 450 (Swings *et al.* 1983). QSOs B and C are separated by only 24″, while Q0118−031A is located 4′.8 from B and 4′.9 from C. Fig. 1 shows the relative locations of the objects and summarizes their basic parameters.

2 Observations

Low dispersion observations of all three QSOs were made using the Image Dissector Scanner attached to the Boller & Chivens spectrograph at the $f/8$ focus of the ESO 3.6-m telescope in 1982 September. Intermediate dispersion spectra of QSOs B and C were obtained in 1983 September using the Image Photon Counting System (IPCS; Boksenberg & Burgess 1973) attached to the Royal Greenwich Observatory spectrograph at the $f/8$ focus of the 3.9-m Anglo–Australian Telescope. Further intermediate dispersion observations of Q0118−031B were obtained at the Multiple Mirror Telescope Observatory in 1983 October, using a photon-counting reticon

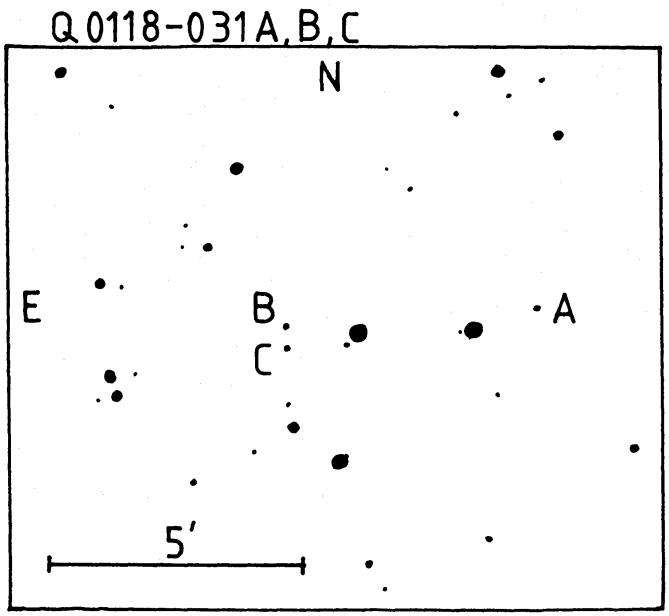

Figure 1. Finding chart for Q0118−031A, B, C (from the Palomar Sky Survey O print). The designations of the objects as given by Swings *et al.* (1983) are 239(A), 240(B) and 241(C). The position of Q0118−031A is α 01 18 20.6 δ −03 08 02 (1950). The projected separations are AB=4′.8≡1.24 Mpc at z_{em}(A)=1.445 (H_o =100 km s^{-1} Mpc^{-1}, Ω=1); AC=4′.9; BC=24″. The B magnitudes were measured from 200 s exposures with the RGO CCD at the prime focus of the AAT on 1983 October 26 and are 18.70(A), 19.01(B) and 19.94(C). The accuracy of these values is ±0.04 mag.

detector on the MMT spectrograph. Finally, further low dispersion observations of Q0118−031A were obtained with the IPCS/RGO spectrograph on the AAT in 1984 August. Table 1 summarizes the observational parameters and the results obtained.

In the 1983 September AAT observations objects B and C were both placed in the slit and observed simultaneously. Wavelength calibration exposures (from a Cu–Ar hollow cathode

Table 1. Journal of observations.

	ESO 1982 September	AAT 1983 September	MMT 1983 October	AAT 1984 August
Observation date	1982 September 18, 19	1983 September 30 and October 1	1983 October 5	1984 August 30
Telescope	ESO 3.6-m	AAT 3.9-m	MMT 4.4-m eq	AAT 3.9-m
Instrument	B & C, IDS	RGO, IPCS	MMT s'graph	RGO, IPCS
Camera focal length (cm)	14.4	25	25	82
Grating 1 mm^{-1}	300	1200	600	250
Dispersion Å mm^{-1}	224	33	27	49
Detector format	2048	2044×60	2048	2040×55
Pixel sizes	4.5 Å	0.50 Å×2″.35	0.40 Å	0.74 Å×1″.4
Slit (arcsec)	4×4	1.8	1.0	1.0
Seeing (arcsec)	5	2	1.3	1.5
Resolution (Å FWHM)	12	1.0–2.0	1.4	3.5
Wavelength range (Å)	3800–7300	3252–4100	4380–5200	3641–5019
Objects observed	A, B, C	B, C	B	A
Total exposure time (min)	30 40 40	170	45	50
Wavelength range (Å)		4075–4922		
Objects observed		B, C		
Total exposure time (min)		113		

lamp) were obtained at 1700 s intervals. For the AAT data the reduction procedure consisted of flat-fielding to remove pixel-to-pixel gain variations in the detector, a weighted sum to combine the object signal in several adjacent spatial increments, linearization of the wavelength scale using comparison spectra, sky subtraction, extinction correction, a weighted sum of separate exposures, and normalization using observations of a standard star to remove variations in instrumental sensitivity with wavelength. These procedures result in spectra whose ordinate is on a relative scale of λF_λ. Finally, all spectra in this paper have been converted to vacuum heliocentric wavelenths. The use of weights in the addition of signals from individual spatial increments and for the combination of separate exposures optimises the signal-to-noise ratio of the resulting spectrum (Robertson 1983). The spectral resolution of the AAT data varies significantly with wavelength, between extremes of 1.0 and 2.1 Å. The mean resolution is 1.6 Å.

The reduction of the ESO and MMT data was similar except that the IDS and reticon collect only two simultaneous spectra (object and sky) so the addition of spectra from adjacent spatial increments does not arise. The spectral resolution of the MMT data is 1.4 Å and that of the ESO data is 12 Å.

3 Emission-line spectra

Composite low dispersion spectra of each object were constructed, using all available data (except the MMT intermediate dispersion observation), and are shown in Figs 2–4. Table 2 lists the wavelengths of the emission lines. The median wavelength (i.e. the wavelength which equally splits the area of the line) is used as the location parameter since it is less affected by noise than the peak value, and less influenced by wings and the exact continuum fit than is the mean (centre of

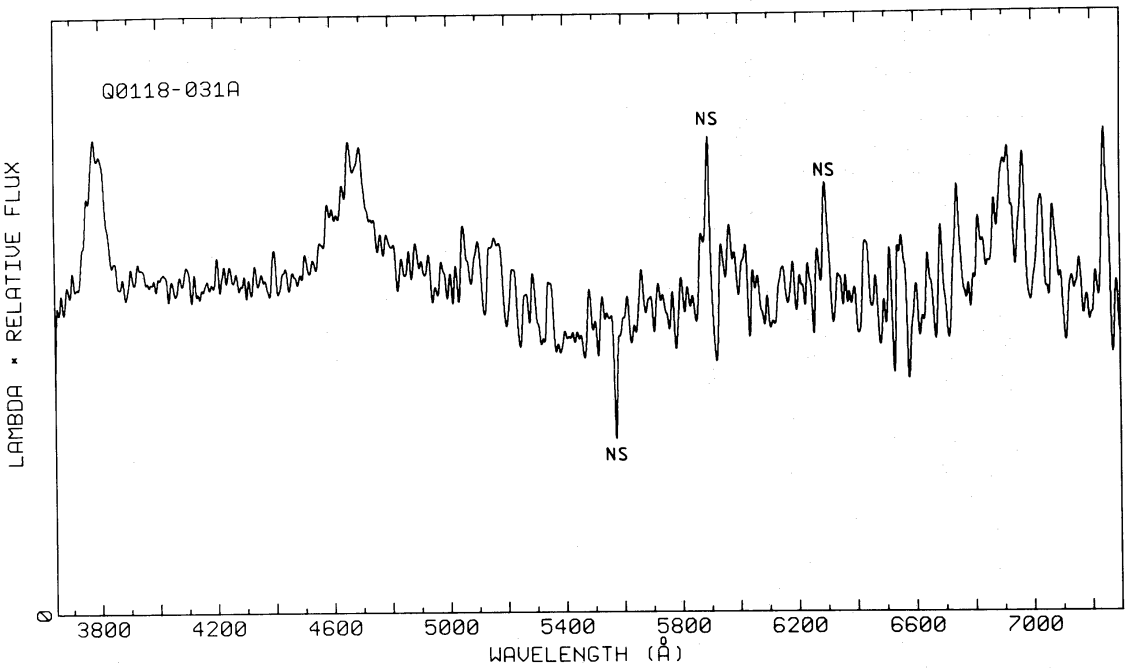

Figure 2. Composite low dispersion spectrum of Q0118–031A. The data used are: (1) AAT 1984 August for λ3641–4350; (2) equal weight mean of AAT 1984 August and ESO 1982 September for λ4351–5019; (3) ESO 1982 September for λ5020–7300. After merging of these segments the data were smoothed with a Gaussian of FWHM 7.7 Å, resulting in a resolution of 8 Å in segment (1), 11 Å in (2) and 14 Å in (3). The ordinate in this spectrum and all others in this paper is a relative scale of λF_λ, and the wavelengths are vacuum heliocentric. Features marked 'NS' are residuals of night sky lines.

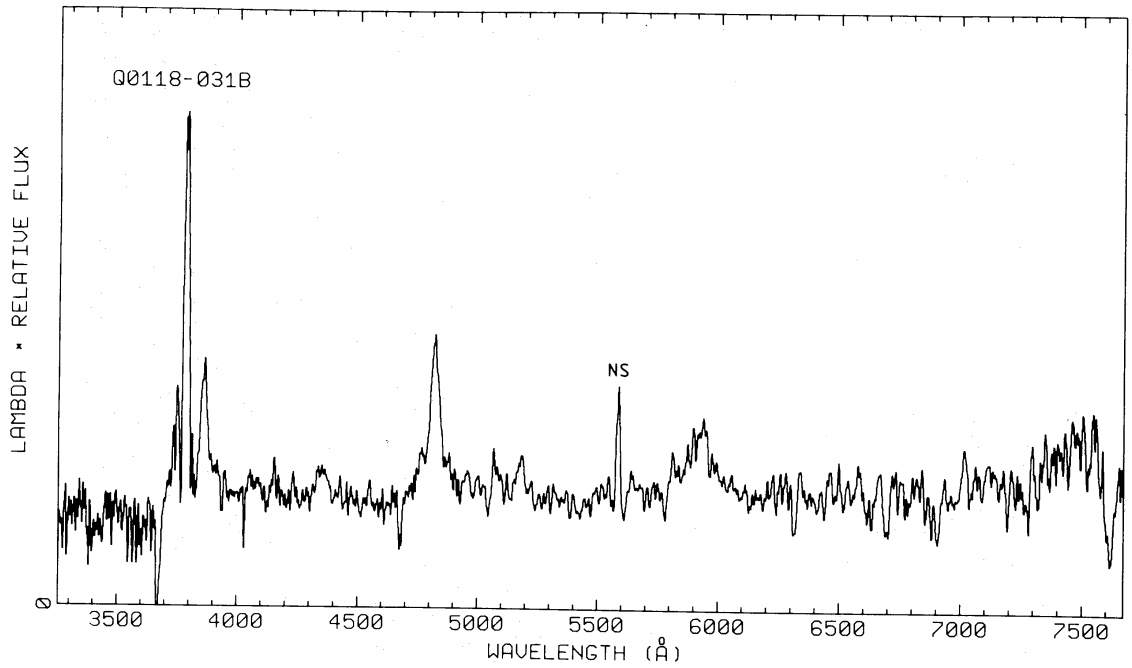

Figure 3. Composite low dispersion spectrum of Q0118−031B. The data used are: (1) AAT 1983 September first wavelength range for λ3254−4099; (2) equal weight mean of AAT 1983 September second wavelength range and ESO 1982 September for λ4100−4922; (3) ESO 1982 September for λ4923−7672. Before plotting, the composite was smoothed with a three-point Gaussian of FWHM 3.6 Å, resulting in a resolution of 4 Å in segment (1). In segment (2) the instrumental profile consists of a broad (13 Å) component with a 4 Å narrow component superimposed. (This is allowable since all features of interest are broader than 13 Å.) In segment (3) the resolution is 13 Å. The feature at λ7600 in this spectrum and in Fig. 4 is a detector artefact.

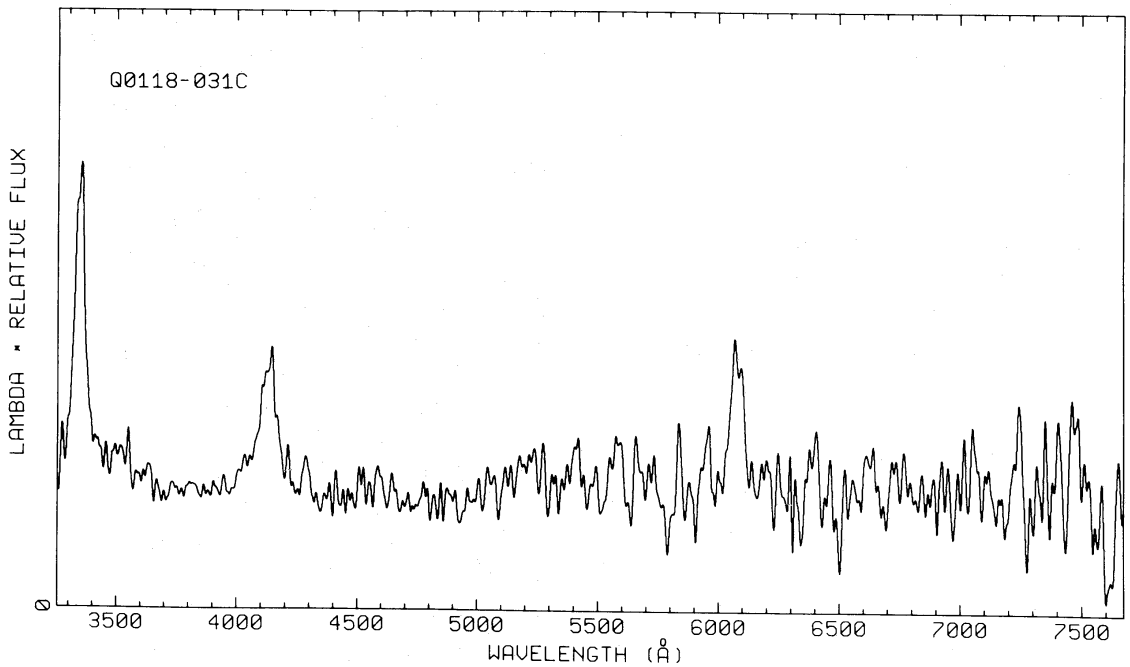

Figure 4. Composite low dispersion spectrum of Q0118−031C. The wavelength segments and data sources are exactly as for Fig. 3. However, after merging, this spectrum was smoothed with a Gaussian of FWHM 9.3 Å, resulting in resolutions of 9 Å in segment (1), 12 Å in (2) and 15 Å in (3).

Table 2. Emission lines.

	Lyα	N v	C iv	He ii	C iii]	Mg ii	Mean†
λ_{rest}	1215.67	1240.13	1549.06	1640.43	1908.73	2798.74	
Q0118−031A λ_{med}*			3786.7		4672.1	6915.7	
z			1.4445		1.4478	1.4710	1.445±0.002
Q0118−031B λ_{med}*	3782.5	3859.6	4821.5		5922.2		
z	2.1114	2.1122	2.1125		2.1027		2.112±0.001
Q0118−031C λ_{med}*			3346.9	3548.6	4133.5	6076.1	
z			1.1606	1.1632	1.1656	1.1710	1.165±0.002

*λ_{med} denotes median wavelength of signal above level = continuum + 1/3 (peak − continuum).
†Mean of redshifts as selected and weighted (see text).

gravity; centroid). Line wings are still a problem in some cases however, as is uncertainty of the continuum level beneath the Lyα and N v lines for Q0118−031B. For these reasons the median wavelengths have been calculated using the signal above a level situated above the continuum, at a value equal to continuum + ⅓ (line peak − continuum). This gives the median wavelength of the main part of the line peak, ignoring the low level wings. It is insensitive to small errors in continuum level (or shape) and estimation of the peak height.

The resulting emission redshifts are also given in Table 2. For Q0118−031A the Mg ii line was ignored due to its low signal-to-noise ratio and large width, and the C iv line was given a weight four times that of C iii] in determining the redshift. For the other two QSOs all lines were used with equal weight. Effective rest wavelengths for the broad line doublets (N v, C iv, C iii] and Mg ii) were taken from Gaskell (1982). The rest wavelength used for He ii is a simple mean of the three components of the multiplet.

4 Absorption-line spectra

Figs 5 and 6 show the intermediate dispersion spectrum of Q0118−031B, derived from the AAT and MMT data. The absorption lines detected are listed in Table 3. In compiling this list the continuum in the vicinity of each line was fitted by a cubic polynomial (in some cases degree 1 or 2 was used if more appropriate), omitting regions containing other absorption lines and iteratively rejecting discrepant points (more than 2.25σ from the fitted curve). The equivalent width of the absorption line was then calculated in the normal way. The wavelengths given are the median wavelength (of the signal below the fitted continuum). The median is used rather than the mean (centroid) because it again is less affected by wings on the line, and because in the case of absorption lines subject to Poisson distributed noise it can be shown that the median has a lower sampling variance than the centroid.

The uncertainties in wavelength and equivalent width have been calculated using a procedure which assesses the noise in the spectrum as a function of wavelength by subtracting suitably scaled independent runs. It allows for object and sky photon shot noise (the latter varies strongly with wavelength), detector noise, and the wavelength variation of instrumental sensitivity and extinction. This method correctly shows the better signal-to-noise ratio for absorption lines seen against the increased continuum provided by a broad emission line. The details of this analysis, as well as the procedure for calculating wavelength and equivalent width uncertainties from the noise spectrum will be published elsewhere. The wavelength uncertainty as given includes a component to allow for the uncertainty in linearization of the wavelength scale (0.12 Å below 4100 Å; 0.09 Å above 4100 Å).

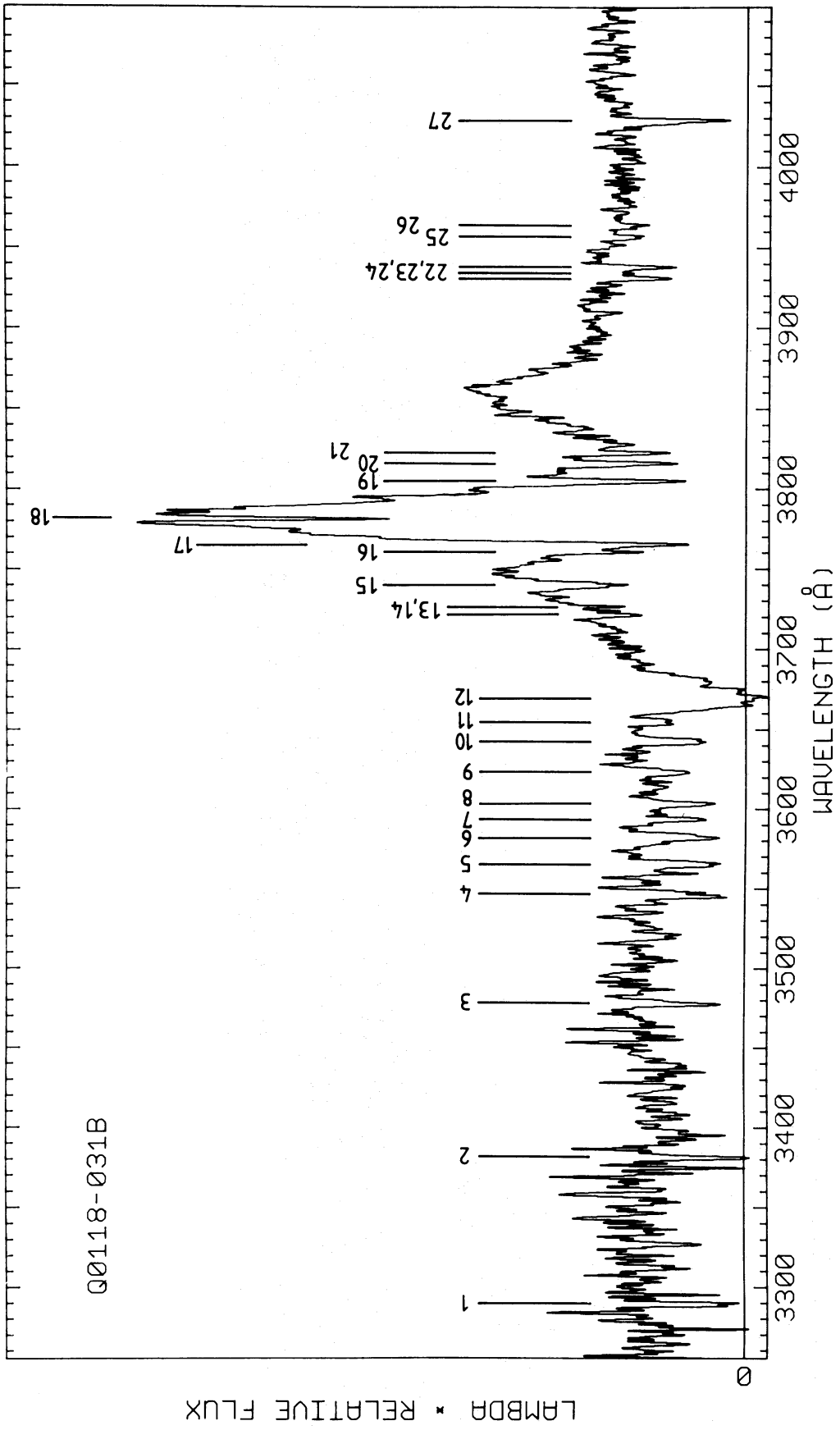

Figure 5. Intermediate dispersion spectrum of Q0118−031B from the first wavelength range of AAT 1983 September data. The data as shown have been smoothed with a three-point Gaussian filter (effective FWHM 0.69 Å), resulting in a final resolution of ~1.8 Å. The absorption lines indicated are listed in Table 3.

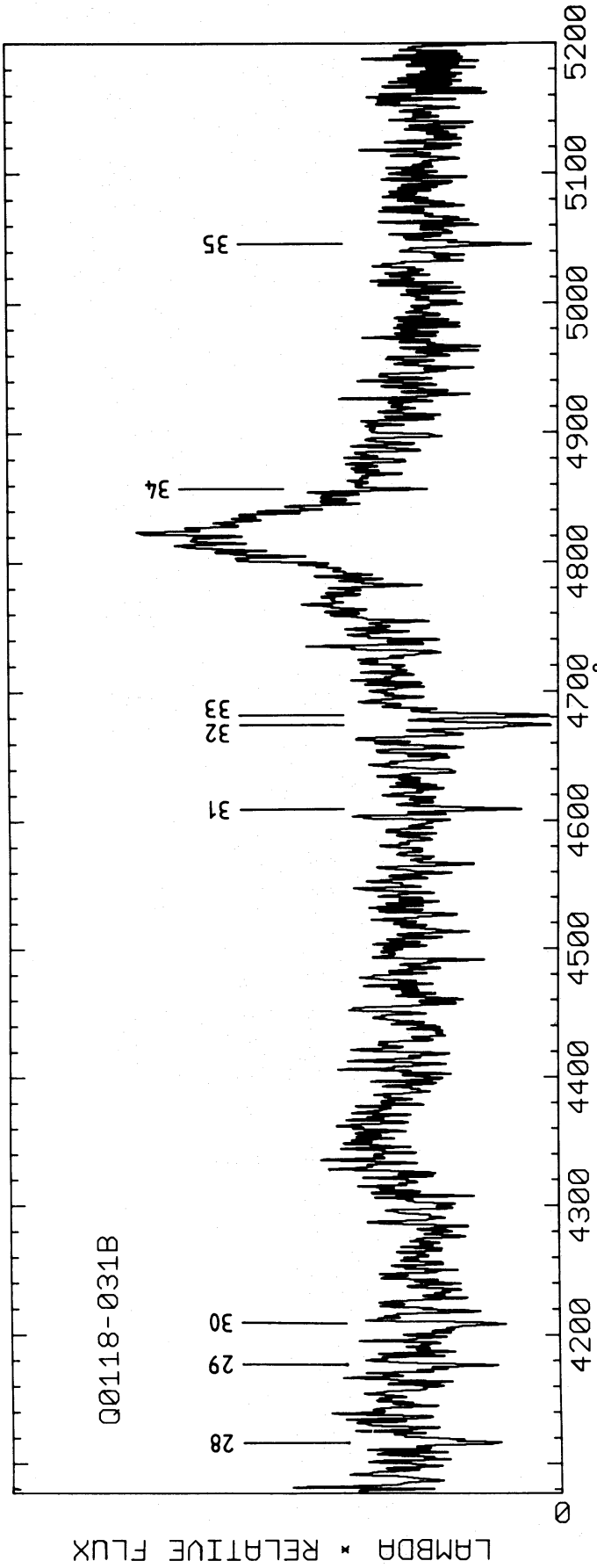

Figure 6. Intermediate dispersion spectrum of Q0118−031B derived from the second wavelength range of the AAT 1983 September data and the MMT data. The data have been merged as follows: (1) λ4075–4380.9: AAT only (2) λ4381.4–4922.5: MMT data used with weight increasing from 0.144 to 0.385 (AAT weight=1–MMT weight), to allow for variation of MMT signal-to-noise ratio with wavelength (3) λ4922.9–5201.5: MMT only. The data as plotted have been smoothed with a three-point Gaussian filter (effective FWHM 0.92 Å), giving a final resolution of ~1.7 Å. The absorption lines indicated are listed in Table 3.

It is important to note that the uncertainties as calculated allow for the statistical aspects of the errors, but cannot include uncertainties in *interpretation*, e.g. whether a line is single or blended with another, and cases where the suitable *form* for the continuum fit is not clear. In such cases a '+' is appended to the error estimate in Table 3 to indicate that the total error will be larger. In the line list (Table 3) a cutoff at 4σ (i.e. $W_\lambda = 4.0\sigma_W$) has been applied.

Where lines can be identified with distinct absorption redshift systems, the ion, vacuum rest wavelength and oscillator strength (f) are given in Table 3. The f values for Si II have been taken from Shull, Snow & York (1981). There are two definite absorption systems, $z_{abs} = 2.0192 \pm 0.0001$ (A) and 1.4648 ± 0.0001 (B). System A is the strongest, with 14 identified lines in the range observed, and a very broad Ly α line (FWHM 18 Å) which indicates a column density sufficient to produce damping wings. The neutral hydrogen column density indicated by the width of this line (Smith, Turnshek & Wolfe 1983) is $\sim 1.4 \times 10^{20}\,\mathrm{cm}^{-2}$. In this absorption system there are five observed lines due to Si II so these have been used to find the best value of the Doppler broadening parameter b, using standard Voigt profile analysis. A good match to the (rest frame) equivalent widths of these lines was obtained with $b = 100\,\mathrm{km\,s}^{-1}$. Using this value for all lines in system A, column densities were calculated from the equivalent widths of the lines. These indicate abundances of ~ 0.1 solar for all detected heavy elements, as is typical for these heavy element absorption systems. This value for abundances relative to hydrogen assumes that essentially all the hydrogen is neutral. This is plausible since a cloud with this hydrogen column is extremely optically thick to ionizing photons. However such a picture may be too simple since carbon exists primarily as C IV in this cloud N(C IV)/N(C II)$\sim$7. If a substantial fraction of the hydrogen is ionized then the heavy element abundances will be less than 0.1 solar.

The Voigt profile modelling of the lines in this system (A) showed that linewidths of $180-240\,\mathrm{km\,s}^{-1}$ (FWHM) are predicted in the rest frame for $b = 100\,\mathrm{km\,s}^{-1}$. This translates to 2.2–3.0 Å observed width, which is expected to be resolved in our intermediate dispersion spectra. Linewidths were calculated from the observed spectra by finding for each line the wavelengths on either side of the median which bound 34 per cent of the total line area between themselves and the median. The width was then calculated as the difference between these two wavelengths multiplied by 1.1775. For a Gaussian profile this gives exactly the FWHM and for any reasonable centrally concentrated profile it gives a result very close to the FWHM. This procedure is more resistant to the effects of spurious noise wings at the edges of the line than is the calculation of widths via the standard deviation. For the nine unblended lines of good signal-to-noise ratio in System A the mean width (after deconvolution to allow for the instrumental broadening) was $200 \pm 20\,\mathrm{km\,s}^{-1}$, entirely consistent with the above prediction. Similarly the model fits to the lines predict that many of the lines will not be black, and this is confirmed in our observations. For example residual intensities equal to 10 per cent of the continuum are predicted for the C IV lines, and 80 per cent (i.e. line depth 20 per cent) for Fe II 1608.46. It is clearly the large velocity dispersion that causes substantial equivalent widths to be observed from relatively unsaturated lines, and indeed causes the lines to be unsaturated with their quite substantial column densities.

The agreement of the line parameters with a Voigt profile model must be fortuitous to a certain extent, since there is no possibility that the value $b = 100\,\mathrm{km\,s}^{-1}$ is thermally produced as assumed in the derivation of the Voigt function (for Si $b = 100\,\mathrm{km\,s}^{-1}$ corresponds to the unreasonable temperature 1.7×10^7 K or $3kT/2 = 2.2$ keV). Instead, it must be largely due to the presence of individual subcomponents (and/or turbulent motions). Subcomponents are suggested by the very asymmetric profile of the C II 1334.53 line and to a lesser extent the Si II 1260.42 line (the asymmetry is not expected to be the same in all lines since different subcomponents will be at different degrees of saturation in different lines). In order to produce the rather good fit to Voigt function models as above the subcomponents must be distributed in velocity in such a way

Table 3. Absorption lines in the spectrum of Q0118−031B.

No.	λ_{obs}(Å)	σ_λ(Å)	W_{obs}(Å)	σ_w(Å)	Identification	f	z_{abs}	Absorption system
1	3289.1	0.4	2.7	0.6	C II	1334.53 0.118	1.4646	B
2	3381.0	0.3	2.7	0.7				
3	3477.8	0.3	2.2	0.4				
4	3545.9	0.3	3.2	0.5				
5	3565.5	0.2	2.9	0.3				
6	3582.0	0.2+	3.2	0.3+				
7	3593.5	0.2	1.7	0.2	Si II	1190.42 0.25	2.0187	A
8	3603.4	0.2	2.4	0.3	Si II	1193.29 0.50	2.0197	A
9	3623.2	0.3	1.7	0.3				
10	3642.7	0.3	2.6	0.3	Si III	1206.51 1.66	2.0192	A
11	3654.9	0.6	1.3	0.3				
12	3671.8	0.3+	20.6	0.5+	H I	1215.67 0.4162	2.0204:	A
13	3721.5	0.2	0.9	0.14				
14	3726.7	0.2	0.44	0.10				
15	3740.2	0.2	1.8	0.2				
16	3760.6	0.17+	1.1	0.11+				
17	3765.3	0.13+	2.4	0.10+	Si II	1526.71 0.23	1.4663	B
18	3781.6	0.14	0.82	0.05+				
19	3804.9	0.15	2.3	0.13	Si II	1260.42 0.96	2.0188	A
20	3816.1	0.16	1.8	0.14	C IV	1548.19 0.194	1.4649	B
21	3822.9	0.16	1.1	0.13	C IV	1550.76 0.0970	1.4652	B
22	3931.6	0.17	1.3	0.11	O I	1302.17 0.0486	2.0194	A
23	3934.9	0.2+	0.37	0.08+	Ca II	3934.78 0.688	0.0000	
24	3938.2	0.17+	1.3	0.13+	Si II	1304.37 0.147	2.0192	A
25	3956.8	0.3	0.6	0.13				
26	3964.2	0.3	0.6	0.13	Fe II	1608.46 0.0963	1.4646	B
27	4028.6	0.15	2.9	0.17	C II	1334.53 0.118	2.0187	A
28	4116.8	0.4	2.8	0.5	Al II	1670.79 1.88	1.4640	B
29	4176.6	0.3	1.6	0.4				
30	4208.3	0.3	2.2	0.4	Si IV	1393.76 0.528	2.0194	A
31	4609.3	0.2	1.8	0.4	Si II	1526.71 0.23	2.0191	A
32	4674.0	0.2	4.2	0.4	C IV	1548.19 0.194	2.0190	A
33	4681.3	0.2	3.5	0.4	C IV	1550.76 0.0970	2.0187	A
34	4856.6	0.2	0.7	0.2	Fe II	1608.46 0.0963	2.0194	A
35	5045.6	0.2	2.1	0.4	Al II	1670.79 1.88	2.0199	A

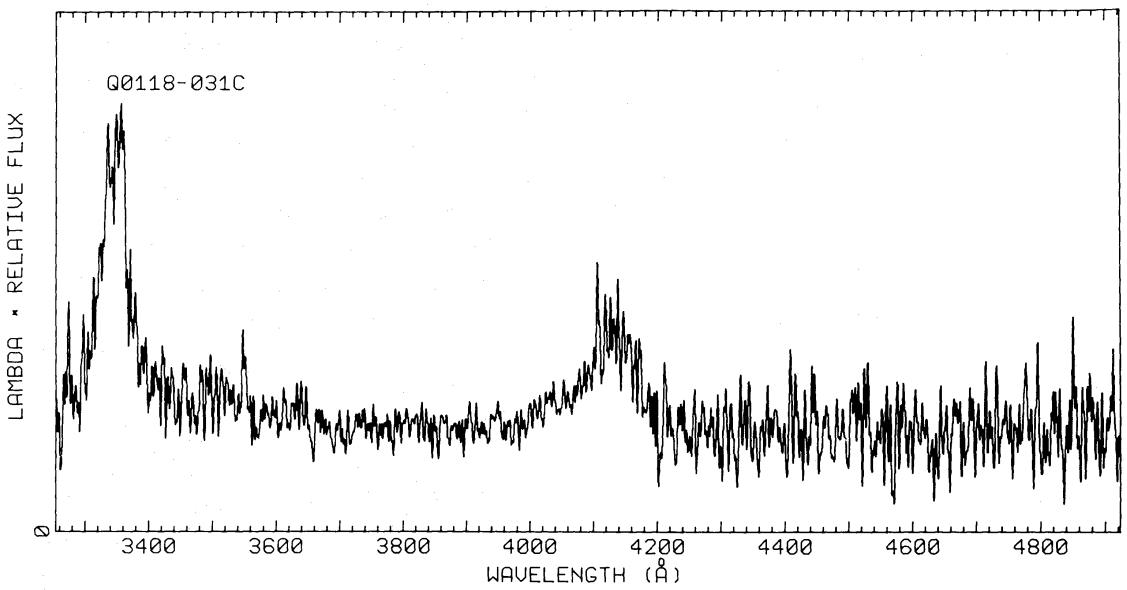

Figure 7. Intermediate dispersion spectrum of Q0118−031C derived from AAT 1983 September first wavelength range (3252–4100 Å) and second wavelength range (4100–4923 Å). The data as plotted have been smoothed to a resolution of 2.5 Å.

as to crudely approximate a Maxwellian distribution of the gas about the dominant rest velocity. This high column density absorption system is similar to a number of other known absorption systems in QSOs (e.g. PHL 957: Coleman *et al.* 1976, PKS 0528+250: Morton *et al.* 1980.) The ionization conditions and column densities are similar to what is expected for a line of sight which intersects the disc of a galaxy; such discs are usually taken to be the source of these systems.

Absorption system (B) in Q0118−031B has six lines in the range observed. The only ion with more than one observed line in this system is C IV, so it has been used to estimate the Doppler b parameter for this system. A value of $b=60\,\mathrm{km\,s^{-1}}$ fits the C IV equivalent widths and gives a column density $N(\mathrm{C\,IV})\sim 3\times10^{14}\,\mathrm{cm^{-2}}$. This b value is also consistent with the observed linewidths, although these lines are not well resolved and the observed widths do not give good independent evidence for this large a b value (as they do for system A above). The observed line depths are also consistent with this b value, when allowance is made for the instrumental resolution. With this b value the column density of C II is $N(\mathrm{C\,II})\sim 7\times10^{15}\,\mathrm{cm^{-2}}$ and the C II 1334.53 line (line No. 1 in Table 3) is expected to have a width of $\sim 220\,\mathrm{km\,s^{-1}}$. This line is indeed well resolved, with a deconvolved width of $190\,\mathrm{km\,s^{-1}}$, in good agreement considering the uncertainty of observed width parameters. In this interpretation the non-zero central

---

Notes to Table 3

12: Damped Lyα line. Probable blend with another Lyα forest line in red wing.
16, 17: Uncertainties increased due to blending.
18: Continuum uncertain due to peak of emission line.
23: Presence of Ca II 3834.78 inferred from depression between lines 22 and 24, which would be clearly resolved if they were the only lines present.
29, 30: Blue wing presumed due to noise and cut off in analysis.
30: Possibly blended with another line (notwithstanding good redshift agreement with system A) since Si IV 1402.77 is not seen.
34: Below 4σ cutoff, but included because of wavelength agreement in definite redshift system.

intensity observed for this line must be ascribed to noise (which is quite reasonable). The high ratio of N(C II)/N(C IV) indicates that this is a very low ionization system; this is supported by the absence of the Si IV λ1393.76, 1402.77 doublet.

Our intermediate dispersion spectrum of Q0118−031C is shown in Fig. 7. No absorption lines were detected above a 4σ limit in the observed wavelength range (3252−4922 Å). This is not surprising since the lower redshift of QSO C excludes the commonly observed strong *UV* resonance lines (e.g. Lyα – C IV) from appearing in absorption in this object, and moreover QSO C is fainter than QSO B so that the signal-to-noise ratio of its spectrum is only ~50 per cent of that for QSO B. (The 4σ limits on W_λ are 1.2–1.6 Å below 4100 Å and 3–4 Å above 4100 Å.)

We have no intermediate dispersion observations of Q0118−031A, and so are unable to look for absorption systems in that object. This is unfortunate since it precludes a search for associated absorption in QSO A at z_{em}(C)=1.165. It would also be desirable to check for absorption in QSO A near its emission redshift (1.445), since this would be common absorption with respect to system (B) in QSO B.

5 Discussion

The results presented above allow us to search for common absorption in QSOs B and C at $z_{abs} \leqslant 1.17$ and associated absorption in QSO B due to material at the same redshift as QSO A or C. Of these possibilities only associated absorption in QSO B at the redshift of QSO A is seen. This refers to the near coincidence of the z_{abs}=1.4648 absorption system in QSO B with the emission redshift z_{em}=1.445 of QSO A. This redshift difference corresponds to a velocity difference of 2400 ± 250 km s^{-1} in the rest frame of the absorber. The projected spatial separation between the absorber and QSO A is 1.2 Mpc. These separations are consistent with the absorption being due to material associated with a galaxy in a cluster which also contains QSO A, although the velocity difference is close to the upper limit of what could be expected in this interpretation. A difference this large or greater between the radial velocities of two independent objects moving in a cluster with a line of sight velocity dispersion of 1000 km s^{-1} (typical of a rich cluster; Danese, de Zotti & Di Tullio 1980) could be expected to occur in about 10 per cent of cases. This percentage could be larger if the cluster is in the process of collapsing or is unusually rich.

However, the true velocity difference between QSO A and the z=1.4648 absorbing cloud in front of QSO B may in fact be considerably less than 2400 km s^{-1}, because Gaskell (1982) has shown that the high ionization emission lines in QSOs are systematically blueshifted by ~600 km s^{-1} relative to the low ionization lines and the narrow lines (when visible); the latter are presumed to indicate the true redshift of the parent object since they in turn agree with the stellar absorption line redshift. This blueshift of high ionization/high excitation lines has also been noted by Allen *et al.* (1982) and Wilkes & Carswell (1982). A recent clear example is given by Briggs *et al.* (1985). The size of this blueshift varies widely between different QSOs; while the mean is 600 km s^{-1}, the maximum known is 2600 km s^{-1} (Gaskell 1982). Since the emission redshift for QSO A was determined from the high ionization lines C IV and C III], it may be too low by ~600 km s^{-1} or more. If so, this would reduce the velocity difference of 2400 km s^{-1} noted above to a value more typical for a cluster of galaxies. The spatial separation is certainly reasonable for two well separated galaxies in a rich cluster [e.g. the radius adopted by Abell (1958) was 1.5 Mpc].

It is clearly important to estimate the probability that this coincidence in absorption and emission redshifts has arisen by chance. Like all *a posteriori* probabilities this is a difficult question; what we can say is that with two absorption systems in QSO B showing C IV

doublets, and assuming that such absorption systems are randomly distributed in redshift (for $z_{abs}<z_{em}$) the probability that one of them will have by chance a redshift within ± 0.02 ($\Delta V = 2400\,\mathrm{km\,s^{-1}}$) of the given z_{em}(A) is ~6 per cent. (The accessible redshift range for C IV doublets in QSO B is 1.13–2.36.) Therefore the probability of chance occurrence of this associated absorption system is not negligible. This will be the case with all systems such as this and the Q1228+076/1228+077 pair (Robertson & Shaver 1983) in which the spatial and velocity separations correspond to what would be expected from a cluster of galaxies. Only observations of many similar pairs will settle definitively the question of the physical reality of such associated absorption. However with two similar cases (this and Q1228+076/1228+077) it is certainly highly plausible.

If we accept the physical reality of this new case of associated absorption, it provides further evidence that (at least some) high redshift absorption systems are due to intervening matter unrelated to the background QSO in which the absorption appears. Regarding the cosmological significance of the redshifts, this case brings the total number of pairs known to show associated absorption to four, while no QSOs have been found in which the low redshift member shows absorption at the emission redshift of the higher redshift member of the pair. As discussed by Shaver & Robertson (1983b) this is strong evidence that redshifts do increase with distance.

It is noteworthy that while we find probable associated absorption in QSO B due to material associated with QSO A 4′.8 away on the sky, there is no associated absorption in B due to C, which is only 24″ away on the sky. It is clear that the material causing associated absorption is patchy, and is certainly not in the form of uniform halos surrounding all QSOs. This is consistent with our positive results for three other associated absorption pairs (Section 1) but negative results for a number of other pairs [Shaver & Robertson 1983b and 1986 (in preparation)].

Observations of associated absorption such as the present case offer a method (albeit indirect) for examining the cluster environments of QSOs at very substantial redshifts. Recent data suggest that low redshift QSOs ($z \leqslant 0.5$) occur preferentially in groups and poor clusters (Stockton 1978; French & Gunn 1983; Yee & Green 1984) while at higher redshifts it is likely that QSOs were often members of richer clusters (Stocke & Perrenod 1981; Margon, Downes & Spinrad 1983). The occurrence of associated absorption is consistent with this view, and if a sufficient number of suitable pairs of QSOs can be observed it should eventually be possible to derive quantitative data regarding the nature of the clusters containing high redshift QSOs.

Acknowledgments

We thank the Australian Time Assignment Committee for allocating AAT observing time and the Multiple Mirror Telescope Observatory for the allocation of MMT time. PAS and JPS acknowledge hospitality extended at the MMT Observatory, and are especially grateful to Dr R. Weymann and Dr F. Chaffee for their assistance in making the observations possible immediately after the Great Flood. JGR thanks Drs A. C. Davenhall and M. Pettini for the use of their software for calculation of column densities and model line profiles from equivalent widths. We thank Dr D. C. Morton for comments on the draft of this paper.

References

Abell, G. O., 1958. *Astrophys. J. Suppl. Ser.*, **3,** 211.

Allen, D. A., Barton, J. R., Gillingham, P. R. & Carswell, R. F., 1982. *Mon. Not. R. astr. Soc.*, **200,** 271.

Boksenberg, A. & Burgess, D. E., 1973. *Proc. Symp. on Astronomical Observations with TV type Sensors,* Univ. B.C.

Briggs, F. H., Turnshek, D. A., Schaeffer, J. & Wolfe, A. M., 1985. *Astrophys. J.*, **293,** 387.

Burbidge, E. M., Smith, H. E., Weymann, R. J. & Williams, R. E., 1977. *Astrophys. J.*, **218,** 1.

Coleman, G., Carswell, R. F., Strittmatter, P. A., Williams, R. E., Baldwin, J., Robinson, L. & Wampler, E. J., 1976. *Astrophys. J.,* **207,** 1.

Danese, L., De Zotti, G. & Di Tullio, G., 1980. *Astr. Astrophys.,* **82,** 322.

French, H. B. & Gunn, J. E., 1983. *Astrophys. J.,* **269,** 29.

Gaskell, C. M., 1982. *Astrophys. J.,* **263,** 79.

Margon, B., Downes, R. A. & Spinrad, H., 1983. *Nature,* **301,** 221.

Morton, D. C., Chen, J. S., Wright, A. E., Peterson, B. A. & Jauncey, D. L., 1980. *Mon. Not. R. astr. Soc.,* **193,** 399.

Robertson, J. G., 1983. '*IPCS Observations of Faint Object Spectra: Optimisation of the Signal-to-Noise Ratio*', Anglo–Australian Observatory AAO UM 11.

Robertson, J. G. & Shaver, P. A., 1983. *Mon. Not. R. astr. Soc.,* **204,** 69P.

Shaver, P. A., Boksenberg, A. & Robertson, J. G., 1982. *Astrophys. J. Lett.,* **261,** L7.

Shaver, P. A. & Robertson, J. G., 1983a. *Astrophys. J. Lett.,* **268,** L57.

Shaver, P. A. & Robertson, J. G., 1983b. *Nature,* **303,** 155.

Shaver, P. A. & Robertson, J. G., 1985. *Mon. Not. R. astr. Soc.,* **212,** 15P.

Shull, J. M., Snow,. T. P. & York, D. G., 1981. *Astrophys. J.,* **246,** 549.

Smith, H. E., Turnshek, D. A. & Wolfe, A. M., 1983. In: '*Quasars and Gravitational Lenses*', Proc. 24th Liege International Astrophysical Colloquium, p. 567.

Stocke, J. T. & Perrenod, S. C., 1981. *Astrophys. J.,* **245,** 375.

Stockton, A., 1978. *Astrophys. J.,* **223,** 747.

Swings, J. P., Arp, H., Surdej, J., Henry, A. & Gosset, E., 1983. In: '*Quasars and Gravitational Lenses*', Proc. 24th Liege International Astrophysical Colloquium, p. 37.

Wilkes, B. J. & Carswell, R. F., 1982. *Mon. Not. R. astr. Soc.,* **201,** 645.

Yee, H. K. C. & Green, R. F., 1984. *Astrophys. J.,* **280,** 79.